Modulation characteristics of graphene-based thermal emitters

Modulation characteristics of graphene-based thermal emitters

Nathan Howard Mahlmeister, Lorreta Maria Lawton, Isaac John Luxmoore, and Geoffrey Richard Nash*

College of Engineering, Mathematics and Physical Sciences, University of Exeter, Exeter EX4 4QF, U.K.

*E-mail: G.R.Nash@exeter.ac.uk

We have investigated the modulation characteristics of the emission from a graphene-based thermal emitter both experimentally and through simulations using finite element method modelling. Measurements were performed on devices containing square multilayer graphene emitting areas, with the devices driven by a pulsed DC drive current over a range of frequencies. Simulations show that the dominant heat path is from the emitter to the underlying substrate, and that the thermal resistance between the graphene and the substrate determines the modulation characteristics. This is confirmed by measurements made on devices in which the emitting area is encapsulated by hexagonal boron nitride.
© 2016 The Japan Society of Applied Physics

Over the last few years, thermal emission from graphene has primarily been used to probe the electronic and thermal properties of graphene-based transistors under bias.[1–6] In monolayer devices, using graphene both exfoliated and grown by chemical vapor deposition (CVD), thermal emission is not spatially uniform and the maximum emission ("hotspot") occurs at the point corresponding to the minimum conductivity, i.e., the charge neutrality point.[1–7] The application of a gate bias, which changes the charge distribution, can be used to move the hotspot along the length of the devices. Recently, we have assessed the potential of using graphene-based thermal emitters to enable the applications of low-cost, intrinsically safe, portable infrared gas sensors in, for example, mine safety.[7] For the currents used, which could be sustained by the devices for over 100 h, the emission from these devices peaked at a wavelength of around 4 µm and covered the characteristic absorption of many important gases, demonstrating the feasibility of developing a graphene-based mid-infrared light-emitting device. Ultimately, such devices could be more cost-effective and sustainable to manufacture than either silicon MEMS or compound semiconductor-based LED alternatives.[8,9]

However, one key advantage of semiconductor LEDs is their ability to be modulated at very high frequencies, which potentially enables both faster response and the use of more sophisticated signal processing approaches. Although a measurable thermal emission was obtained from graphene devices when the drive current was modulated up to a frequency of 100 kHz, the amount of signal (corresponding to the difference between the thermal emission obtained when the current is on and off) measured at 100 kHz was approximately a factor of 100 smaller than that measured at 1 kHz.[7] In this study, we investigate the dependence of thermal emission over a range of drive current frequencies for multilayer graphene-based thermal emitters, both experimentally and by COMSOL finite element simulation.

Multilayer graphene (MLG; from Graphene Square and Graphene Supermarket), pre-transferred on 300-nm-thick SiO$_2$ on a highly p-doped Si substrate, was used to fabricate devices. Electron beam lithography followed by reactive ion etching in an O$_2$/Ar plasma were used to define 600×500 µm^2 areas of graphene. Source and drain contacts, 600 µm

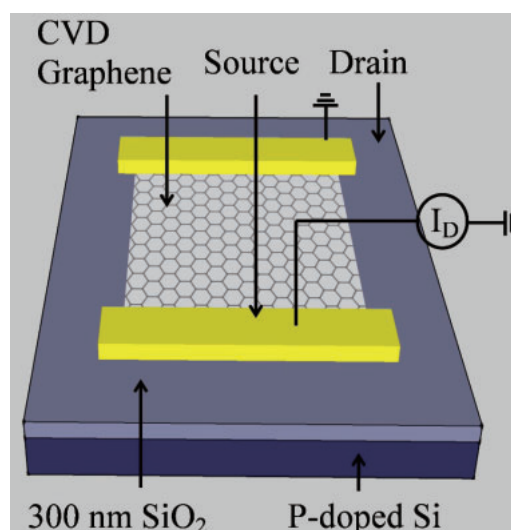**Fig. 1.** Schematic diagram of a large-area CVD graphene infrared emitter.

long and 200 µm wide, of Cr/Au (7/70 nm) were deposited on graphene by thermal evaporation, resulting in an exposed graphene area of 500×500 µm^2. Figure 1 shows a schematic of a typical device. The uniformity and nature of the graphene were confirmed by Raman spectroscopy, which indicated that multilayer samples contained 3–6 layers of graphene. For electrical characterization and thermal emission measurements the devices were mounted on a ceramic chip holder, and placed inside a vacuum chamber with a CaF$_2$ window for optical access. The vacuum chamber was evacuated to ∼10^{-5} mbar. For all measurements, a pulsed DC current with a 50% duty cycle was applied using a Keithley 6221 current source. A two-terminal current–voltage measurement was used to obtain the resistance of the device, which was typically around 1300 Ω/□, at room temperature, with the resistance due to the contacts and leads assumed to be negligible. The resistance is typical of those obtained using CVD graphene.[10] Spatial emission measurements were performed by collecting the emitted light using a reflecting objective lens (NA = 0.28) and then focusing the light using a CaF$_2$ lens onto a liquid-nitrogen-cooled MgCdTe detector, with a 2–12 µm response. The reflecting objective, CaF$_2$ lens, and detector were mounted on an *xy*-stage and the spatial
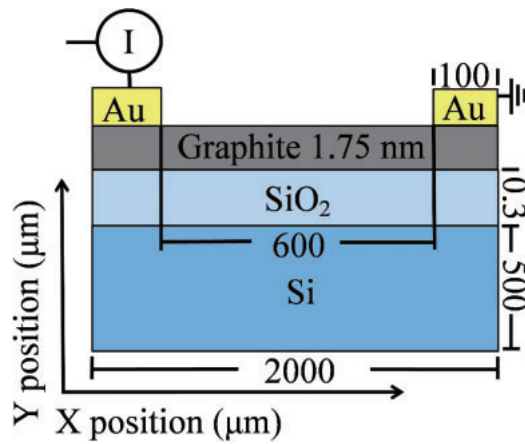
Fig. 2. Example of the geometry simulated using COMSOL.

Fig. 3. (a) Spatially resolved thermal emission plot of the multilayer device. The black line indicates the data taken for the 1D plot. (b) Simulated normalized temperature profile along the surface of COMSOL model at 1 kHz compared with the normalized measured intensity across the center of the multilayer device.

variation of the thermal emission was measured by scanning the microscopy system over the sample. A low-noise preamplifier was used to amplify the signal from the detector before it passed to a lock-in amplifier for phase-sensitive measurement. Spatial measurements were performed using peak injection currents on the order of tens of milliamps at 1 kHz. The total thermal emission from the device was also measured over a range of drive current frequencies, where a CaF_2 lens, rather than the objective, was used to collect the emission from the device. The drive current frequency ranged from 1 to 100 kHz (the limit of the current source), in contrast to previous measurements where only DC or pulsed DC drive currents at a set frequency were used.[2–4,7] In these optical measurements, the signal measured with the lock-in amplifier corresponds to the difference in emission with and without current flowing through the graphene.

COMSOL was previously used to simulate the heat transfer in suspended graphene flakes and graphene heat sink structures.[11,12] In this work, a two-dimensional (2D) time-dependent model was set up, as schematically shown in Fig. 2, combining both the heat transfer in solids and electric current modules. This allowed the Joule heating of graphene to be simulated. Thin graphite, approximately 5 layers, with its cross-plane thermal conductivity (along the c-axis) set to be 6 W·m^{-1}·K^{-1}, which is the cross-plane thermal conductivity of bulk graphite, was used, while the in-plane thermal conductivity was taken to be 2000 W·m^{-1}·K^{-1}.[13,14] The resistance of the thin graphite was set to be 1300 Ω/□, the measured value for the multilayer device. Two different uniform values for the interface thermal resistance R_t between graphite and SiO_2 were implemented in the model. The first value was set at 2×10^{-8} m^2·K·W^{-1}, which is equivalent to the thermal resistance of ~25 nm for SiO_2 and was extracted from measurements of exfoliated devices. A second higher value of 2×10^{-7} m^2·K·W^{-1} [15–18] was also chosen to reflect that there will be areas of CVD graphene in good contact with the substrate, with little to no thermal resistance, and areas with poor or no contact with the substrate, where thermal resistance is much higher. This is due to wrinkles, ripples, and holes produced by CVD growth and transfer processes.[19,20] It was assumed that the emissivity of few-layer graphene is 6%, and that the base of the substrate is thermally anchored to the sample holder and remains at room temperature.[7]
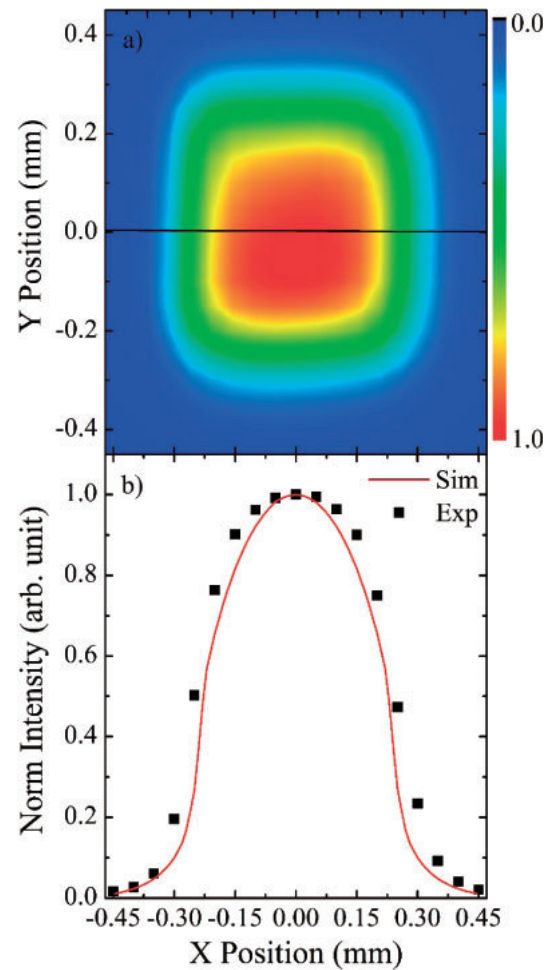
The measured spatial variation of the thermal emission from a typical multilayer device for a peak current density of 1.0×10^7 A·cm^{-2}, well below the breakdown current of graphene, at a drive frequency of 1 kHz is shown in Fig. 3(a).[21] In contrast to that from monolayer graphene-based devices, the thermal emission from multilayer devices has a maximum intensity at the center of the emitting area, as might be expected from a conventional semimetal filament. The emission intensity as a function of position across the center of the device is shown in Fig. 3(b), where the intensities have been normalized to the peak intensity at the center of the device. Simulated normalized intensities obtained from the COMSOL model are also shown in Fig. 3(b). These were obtained by first extracting the temperature of the emitting area as a function of position across the emitting area with the current on or off. Using the extracted temperatures and assuming that the emission is that of a grey body, we calculated the measured intensity using the known spectral response of the detector. Overall, there is good agreement between the measured and simulated results, demonstrating the validity of the COMSOL model.

To investigate the modulation characteristics of the graphene-based emitter, the emission from the devices was simulated as well as measured as a function of drive fre-
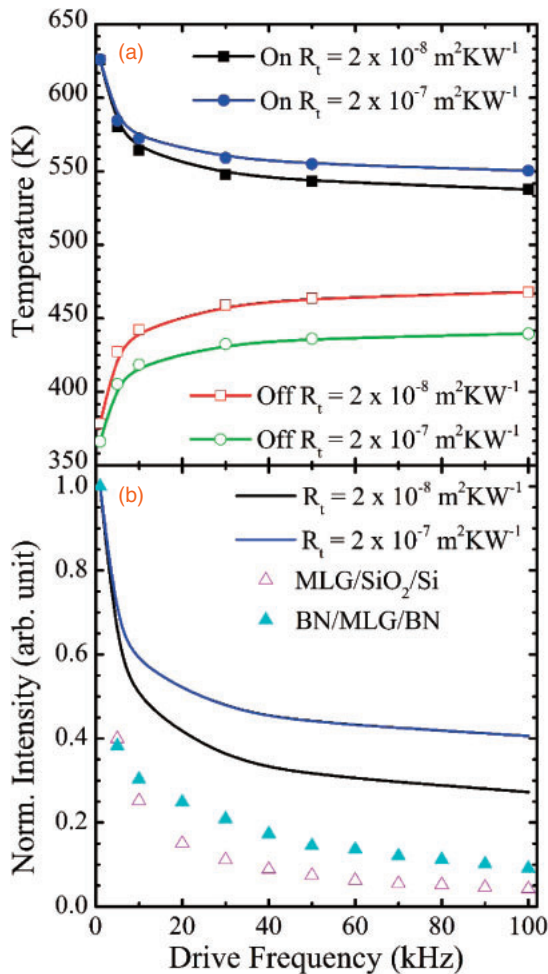
Fig. 4. (a) Simulated on and off temperatures at equilibrium for two different thermal resistances between graphite and SiO₂. Lines are guides for the eye and not fitted curves. (b) Measured, open and closed triangles; calculated from simulations, blue and black lines; normalized emission intensity as a function of frequency. Simulations include two different thermal resistances between thin graphite and SiO₂.

quency at a current density of $1.2 \times 10^7 \, \text{A·cm}^{-2}$. In Fig. 4(a), the temperatures of the center of the emitting area extracted using the COMSOL model are plotted as a function of the drive frequency for the two different thermal resistances between graphene and the underlying silicon dioxide. For both thermal resistances, the highest on-temperature and the lowest off-temperature occur at a frequency of 1 kHz (corresponding to a pulse width of 1 ms). The on-temperature decreases with increasing frequency, suggesting that, as the pulse width is reduced, the time during one pulse becomes insufficient to fully heat the graphene. The on-temperature is higher across the frequency range in the case of higher thermal resistance, as might be expected as heat flow down into the substrate is the dominant thermal path.[4,5,13,22,23] In contrast, the off-temperature in both cases increases with increasing frequency, as for short pulses, there is insufficient time for the heat to fully dissipate before the current is switched on again. Somewhat counterintuitively, higher temperatures are obtained in the case of low thermal resistance. However, this can be explained by the fact that the lower thermal resistance between graphene and silicon dioxide leads to an overall increase in substrate/off temperature. In a real system, for example, a gas sensor, what is important is

the available modulated intensity and these simulations illustrate some of the complexity in designing a real device.

The emission intensities were extracted from the simulated temperatures by again assuming that the emission from graphene is that of a grey body, and they are plotted as a function of frequency in Fig. 4(b). From the simulated intensities, it is clear that increasing the thermal resistance between the MLG emitter and the underlying SiO₂ causes an increase in the intensity, with an approximate increase of 1.5-fold above the frequency of 30 kHz. The measured values of emission at a current density of $2.0 \times 10^7 \, \text{A·cm}^{-2}$ are also plotted in Fig. 4(b), where the open triangles correspond to the emission from the MLG device. The measured intensity drops rapidly as a function of frequency, but is approximately 5-fold lower than those obtained from the simulations across the frequency range.

However, it is more instructive not to compare the measured and simulated values, but to explore the consequences of experimentally increasing the thermal resistance between the MLG emitter and the underlying substrate. The closed symbols in Fig. 4(b) therefore correspond to the measured intensity obtained from a new device in which the multilayer graphene is encapsulated above and below by multilayer hexagonal boron nitride.[24] Hexagonal boron nitride (h-BN) makes for a good dielectric support for graphene owing to its clean, atomically smooth surface and the fact that it belongs to the same hexagonal layered family as graphene and has a similar lattice constant. In comparison with multilayer graphene on SiO₂, the thermal emission from MLG on multilayer h-BN increases by a factor of 2 at high frequencies (≥30 kHz). This can be explained by considering that the anisotropy of the thermal conductivity of h-BN is due to its layered crystal structure with a c-axis thermal conductivity of $\sim 2 \, \text{W·m}^{-1}\text{·K}^{-1}$.[25] In the basal plane, the thermal conductivity has been shown to be $\sim 400 \, \text{W·m}^{-1}\text{·K}^{-1}$ at room temperature.[26] As heat loss from the graphene is dominated by the vertical heat sinking path, the anisotropy of the thermal conductivity has a marked effect on the modulation characteristics of the device. Taking the thickness of the bottom multilayer h-BN to be $\sim 13 \, \text{nm}$ and the interface thermal resistance per unit area to be $1.35 \times 10^{-7} \, \text{m}^2\text{·K·W}^{-1}$ for the graphene/h-BN interface and $2.2 \times 10^{-8} \, \text{m}^2\text{·K·W}^{-1}$ for the h-BN/SiO₂ interface, the additional thermal resistance per unit area for the h-BN device is calculated to be $1.435 \times 10^{-7} \, \text{m}^2\text{·K·W}^{-1}$ relative to graphene/SiO₂ devices with an interface thermal resistance of $\sim 2 \times 10^{-8} \, \text{m}^2\text{·K·W}^{-1}$ (derived from the value obtained for exfoliated samples.[17,27]). Increasing the thermal vertical resistance in the experiments therefore leads to an increase in the measured intensity at high frequencies, in agreement with the results of COMSOL simulations where the interface thermal resistance was increased by a similar amount. Further optimization of the device design should enable the emission intensity at higher frequencies to be further increased.

In summary the thermal modulation as a function of drive frequency for large-area CVD graphene devices was investigated experimentally and simulated by finite element method modelling in COMSOL. For devices with a multilayer graphene emitter, a measurable modulation was observed at 100 kHz, but the measured intensity was approximately 100-fold less than that measured at 1 kHz. COMSOL

simulations showed that the measured intensity at high frequencies can be increased by increasing the thermal resistance between the graphene emitter and the underlying SiO_2. Measurements showed that the encapsulation of the emitting area with hexagonal boron nitride can increase the thermal resistance. This approach therefore provides a promising route to the realization of practical infrared emitters that can be used to replace expensive semiconductor LED equivalents.

1) M.-H. Bae, Z.-Y. Ong, D. Estrada, and E. Pop, Nano Lett. **10**, 4787 (2010).
2) M.-H. Bae, S. Islam, V. E. Dorgan, and E. Pop, ACS Nano **5**, 7936 (2011).
3) M. Freitag, H.-Y. Chiu, M. Steiner, V. Perebeinos, and P. Avouris, Nat. Nanotechnol. **5**, 497 (2010).
4) K. L. Grosse, M.-H. Bae, F. Lian, E. Pop, and W. P. King, Nat. Nanotechnol. **6**, 287 (2011).
5) M. Freitag, M. Steiner, Y. Martin, V. Perebeinos, Z. Chen, J. C. Tsang, and P. Avouris, Nano Lett. **9**, 1883 (2009).
6) I. J. Luxmoore, C. Adlem, T. Poole, L. M. Lawton, N. H. Mahlmeister, and G. R. Nash, Appl. Phys. Lett. **103**, 131906 (2013).
7) L. M. Lawton, N. H. Mahlmeister, I. J. Luxmoore, and G. R. Nash, AIP Adv. **4**, 087139 (2014).
8) M. Parameswaran, A. M. Robinson, D. L. Blackburn, M. Gaitan, and J. Geist, IEEE Electron Device Lett. **12**, 57 (1991).
9) G. R. Nash, H. L. Forman, S. J. Smith, P. B. Robinson, L. Buckle, S. D. Coomber, M. T. Emeny, N. T. Gordon, and T. Ashley, IEEE Sens. J. **9**, 1240 (2009).
10) X. Li, Y. Zhu, W. Cai, M. Borysiak, B. Han, D. Chen, R. D. Piner, L. Colombo, and R. S. Ruoff, Nano Lett. **9**, 4359 (2009).
11) S. Subrina and D. Kotchetkov, J. Nanoelectron. Optoelectron. **3**, 249 (2008).
12) S. Subrina, J. Nanoelectron. Optoelectron. **8**, 317 (2013).
13) E. Pop, V. Varshney, and A. K. Roy, MRS Bull. **37** [12], 1273 (2012).
14) S. Chen, A. L. Moore, W. Cai, J. W. Suk, J. An, C. Mishra, C. Amos, C. W. Magnuson, J. Kang, L. Shi, and R. S. Ruoff, ACS Nano **5**, 321 (2011).
15) Y. K. Koh, M.-H. Bae, D. G. Cahill, and E. Pop, Nano Lett. **10**, 4363 (2010).
16) K. F. Mak, C. H. Lui, and T. F. Heinz, Appl. Phys. Lett. **97**, 221904 (2010).
17) Z. Chen, W. Jang, W. Bao, C. N. Lau, and C. Dames, Appl. Phys. Lett. **95**, 161910 (2009).
18) L. A. Jauregui, Y. Yue, A. N. Sidorov, J. Hu, Q. Yu, G. Lopez, R. Jalilian, D. K. Benjamin, D. A. Delkd, W. Wu, Z. Liu, X. Wang, Z. Jiang, X. Ruan, J. Bao, S. S. Pei, and Y. P. Chen, ECS Trans. **28** [5], 73 (2010).
19) S. J. Chae, F. Güneş, K. K. Kim, E. S. Kim, G. H. Han, S. M. Kim, H.-J. Shin, S.-M. Yoon, J.-Y. Choi, M. H. Park, C. W. Yang, D. Pribat, and Y. H. Lee, Adv. Mater. **21**, 2328 (2009).
20) N. Liu, Z. Pan, L. Fu, C. Zhang, B. Dai, and Z. Liu, Nano Res. **4**, 996 (2011).
21) S. Hertel, F. Kisslinger, J. Jobst, D. Waldmann, M. Krieger, and H. B. Weber, Appl. Phys. Lett. **98**, 212109 (2011).
22) A. D. Liao, J. Z. Wu, X. Wang, K. Tahy, D. Jena, H. Dai, and E. Pop, Phys. Rev. Lett. **106**, 256801 (2011).
23) I. Jo, I.-K. Hsu, Y. J. Lee, M. M. Sadeghi, S. Kim, S. Cronin, E. Tutuc, S. K. Banerjee, Z. Yao, and L. Shi, Nano Lett. **11**, 85 (2011).
24) H. Barnard, E. Zossimova, L. M. Lawton, N. M. Mahlmeister, I. J. Luxmoore, and G. R. Nash, in preparation for publication.
25) A. Simpson and A. D. Stuckes, J. Phys. C **4**, 1710 (1971).
26) E. K. Sichel, R. E. Miller, M. S. Abrahams, and C. J. Buiocchi, Phys. Rev. B **13**, 4607 (1976).
27) Y. Ni, J. Jiang, E. Meletis, and T. Dumitrică, Appl. Phys. Lett. **107**, 031603 (2015).